Vietnam Journal of Mechanics, VAST, Vol. 41, No. 3 (2019), pp. 217 – 231
DOI: https://doi.org/10.15625/0866-7136/13673

BUCKLING AND POSTBUCKLING OF CNT-REINFORCED COMPOSITE SANDWICH CYLINDRICAL PANELS SUBJECTED TO AXIAL COMPRESSION IN THERMAL ENVIRONMENTS

Hoang Van Tung[1,*], **Vu Thanh Long**[2]
[1]*Hanoi Architectural University, Vietnam*
[2]*University of Transport Technology, Hanoi, Vietnam*
[*]E-mail: hoangtung0105@gmail.com

Received: 10 March 2019 / Published online: 24 June 2019

Abstract. An analytical investigation on the buckling and postbuckling behavior of carbon nanotube reinforced composite (CNTRC) sandwich cylindrical panels exposed to thermal environments and subjected to uniform axial compression is presented in this paper. Beside sandwich model with CNTRC face sheets in the literature, the present work suggests a sandwich model with CNTRC core layer and homogeneous face sheets. Carbon nanotubes (CNTs) are reinforced into matrix phase through uniform or functionally graded distributions. Effective properties of nanocomposite layers are determined according to extended rule of mixture. Formulations are based on the first order shear deformation theory taking into account Von Karman-Donnell nonlinearity. Approximate solutions are assumed to satisfy simply supported boundary conditions and Galerkin method is used to derive the closed-form expression of nonlinear load-deflection relation from which buckling loads and postbuckling paths are determined. Numerical examples are carried out and interesting remarks are given.

Keywords: CNT-reinforced composite; cylindrical panel; sandwich models; buckling and postbuckling.

1. INTRODUCTION

Numerous studies of material scientists have demonstrated unprecedentedly wonderful mechanical, thermal and electrical properties of carbon nanotubes (CNTs) [1–3]. In addition to these superior properties, CNTs possess extremely large aspect ratio. Accordingly, CNTs are ideally used as advanced fillers into isotropic matrix phase to form carbon nanotube reinforced composite (CNTRC) known as a new class of nanocomposites. CNTs and their nanocomposites have huge potential for current and expected applications in many engineering fields, especially in aerospace science and engineering [4].

Shen's propositional work on functionally graded carbon nanotube reinforced composite (FG-CNTRC) [5] has motived studies on static and dynamic responses of structural components made of FG-CNTRC. Based on the first order shear deformation theory (FSDT) and a numerical approach, Liew and co-workers [6–9] investigated linear buckling of FG-CNTRC plates under mechanical loads. Linear buckling of FG-CNTRC plates under mechanical and thermal loads has been dealt with in works of Kiani and coauthor [10–13] employing Ritz method. Based on some approaches, postbuckling behavior of FG-CNTRC plates have been addressed in works [14–19].

Cylindrical panel is major component in many structural applications, especially in aerospace engineering. Macias et al. [20, 21] used finite element method to study linear buckling and postbuckling of FG-CNTRC cylindrical panel under axial compression. Using asymptotic solutions and a perturbation technique, Shen and his collaborator [22–25] presented the results of postbuckling analyses for FG-CNTRC cylindrical panels subjected to mechanical and thermal loading conditions. Based on an analytical approach, Tung and Trang [26–28] examined the nonlinear stability of FG-CNTRC cylindrical panels under mechanical and thermomechanical loads.

Due to advanced characteristics, sandwich structures are widely used in various fields. Vibration response of CNTRC sandwich plates has been addressed in works [29–31] using some different methods. Shen and Zhu [32] made use of a perturbation technique to analyze postbuckling behavior of CNTRC sandwich plates under compressive and thermal loads. Thermal postbuckling analysis for CNTRC sandwich plates has been carried out by Kiani [33] utilizing Chebyshev-Ritz method. In aforementioned works [29–33], sandwich plates are constructed from isotropic homogeneous core layer and CNTRC face sheets. Beside this model of CNTRC sandwich plate, another model of sandwich plate with CNTRC core layer and homogeneous face sheets has been suggested in recent works of Long and Tung [34, 35]. These works indicated that sandwich plate model with CNTRC core layer and thin homogeneous face sheets can give high efficiency of buckling resistance and postbuckling load carrying capabilities. To the best of authors' knowledge, there is no investigation on the nonlinear stability of CNTRC sandwich cylindrical panels under axial compression.

As an extension of previous works on thin CNTRC cylindrical panel and shell [36, 37], this paper presents an analytical study on the buckling and postbuckling behavior of shear deformable CNTRC sandwich cylindrical panels subjected to uniform axial compression in thermal environments. Two sandwich models corresponding to CNTRC face sheets and core layer are considered. Effective elastic moduli of CNTRC layers are estimated according to extended rule of mixture. Formulations are based on the first order shear deformation theory taking into account Von Karman-Donnell nonlinearity. Analytical solutions are assumed and Galerkin method is applied to derive the closed-form expression of load-deflection relation from which buckling loads and postbuckling paths are determined.

2. TWO MODELS OF CNTRC SANDWICH CYLINDRICAL PANEL

Consider a cylindrical sandwich panel of axial length a, length of arc b, radius of curvature R and total thickness h. The panel is reinforced by CNTs and defined in a

coordinate system xyz origin of which is located at a corner on the middle surface, x and y axes are in axial and circumferential directions, respectively, and z axis is perpendicular to the middle surface as shown in Fig. 1.

The sandwich panel is constructed from two face sheets separated by a thicker core layer made of homogeneous or CNTRC materials. It is assumed that core layer and face sheets are perfectly bonded and thickness of each face sheet is h_f. The present study considers two different models of sandwich panels corresponding to CNTRC and homogeneous face sheets and referred to herein as sandwich panels of type A and type B, respectively.

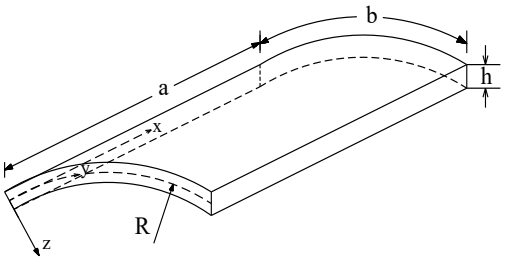

Fig. 1. Configuration and coordinate system of a cylindrical panel

2.1. Sandwich panel of type A: homogeneous core layer and CNTRC face sheets

In this type of sandwich panel, the core layer is isotropic homogeneous and face sheets are reinforced by CNTs as shown in Fig. 2 in which $h_0 = -h/2$, $h_1 = -h/2 + h_f$, $h_2 = h/2 - h_f$, $h_3 = h/2$. The volume fractions V_{CNT} of CNTs in face sheets corresponding to uniform distribution (UD) and four different types of functionally graded (FG) distributions named as FG-X, FG-Λ, FG-V and FG-O are given in the works [34, 35] and omitted here for the sake of brevity.

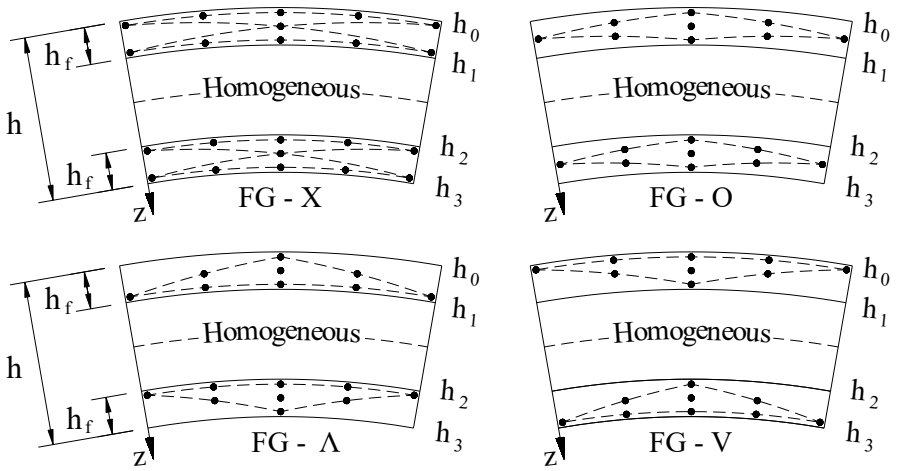

Fig. 2. Functionally graded (FG) types of CNT distribution in sandwich panel of type A

2.2. Sandwich panel of type B: CNTRC core layer and homogeneous face sheets

For sandwich panels of type B, the core layer is reinforced by CNTs and face sheets are isotropic homogeneous as illustrated in Fig. 3.

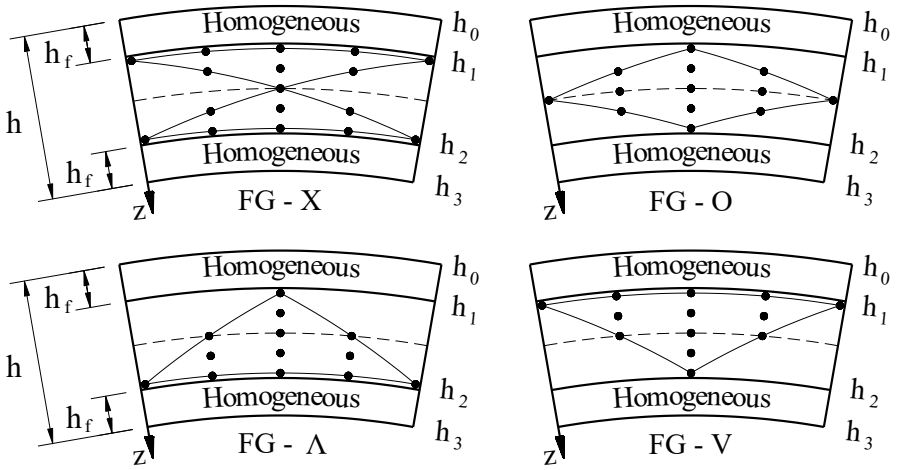

Fig. 3. Functionally graded (FG) types of CNT distribution in sandwich panel of type B

The volume fractions V_{CNT} of CNTs in core layer ($h_1 \leq z \leq h_2$) corresponding to UD, FG-X, FG-Λ, FG-V and FG-O types of CNT distribution are given as follows

$$V_{CNT} = \begin{cases} V^*_{CNT} & \text{UD} \\ 4\dfrac{|z|}{h_2 - h_1} V^*_{CNT} & \text{FG-X} \\ 2\dfrac{z - h_1}{h_2 - h_1} V^*_{CNT} & \text{FG-}\Lambda \\ 2\dfrac{h_2 - z}{h_2 - h_1} V^*_{CNT} & \text{FG-V} \\ 2\left(1 - \dfrac{2\,|z|}{h_2 - h_1}\right) V^*_{CNT} & \text{FG-O} \end{cases} \tag{1}$$

In this study, the properties of constituents are assumed to be temperature dependent and effective elastic moduli E_{11}, E_{22}, G_{12} of CNTRC are determined according to extended rule of mixture as [5, 14]

$$E_{11} = \eta_1 V_{CNT} E^{CNT}_{11} + V_m E^m, \tag{2a}$$

$$\frac{\eta_2}{E_{22}} = \frac{V_{CNT}}{E^{CNT}_{22}} + \frac{V_m}{E^m}, \tag{2b}$$

$$\frac{\eta_3}{G_{12}} = \frac{V_{CNT}}{G^{CNT}_{12}} + \frac{V_m}{G^m}. \tag{2c}$$

Effective Poisson ratio ν_{12} of CNTRC is assumed to be position and temperature independent and is determined as

$$\nu_{12} = V^*_{CNT} \nu^{CNT}_{12} + (1 - V^*_{CNT}) \nu^m. \tag{3}$$

Subsequently, effective thermal expansion coefficients α_{11}, α_{22} of CNTRC layers in the longitudinal and transverse directions have the form as [13,24,33]

$$\alpha_{11} = \frac{V_{CNT}E_{11}^{CNT}\alpha_{11}^{CNT} + V_m E^m \alpha^m}{V_{CNT}E_{11}^{CNT} + V_m E^m}, \tag{4a}$$

$$\alpha_{22} = \left(1+\nu_{12}^{CNT}\right) V_{CNT}\alpha_{22}^{CNT} + \left(1+\nu^m\right) V_m \alpha^m - \nu_{12}\alpha_{11}. \tag{4b}$$

In the Eqs. (1)÷(2c), the specific definitions of V_{CNT}^*, V_m, E_{11}^{CNT}, E_{22}^{CNT}, G_{12}^{CNT}, E^m, G^m,η_1, η_2, η_3, ν_{12}^{CNT}, ν^m, α_{11}^{CNT}, α_{22}^{CNT} and α^m have been given in many previous works on CNTRC structures, for examples [5, 10–15, 23–33], and are omitted here for the sake of brevity.

3. FORMULATIONS

In the present study, the sandwich panels are assumed to be geometrically perfect and moderately thick, and the first order shear deformation theory (FSDT) is used to establish governing equations. Based on the FSDT, strain components are expressed as

$$\begin{pmatrix} \varepsilon_x \\ \varepsilon_y \\ \gamma_{xy} \end{pmatrix} = \begin{pmatrix} \varepsilon_x^0 \\ \varepsilon_y^0 \\ \gamma_{xy}^0 \end{pmatrix} + z \begin{pmatrix} \varepsilon_x^1 \\ \varepsilon_y^1 \\ \gamma_{xy}^1 \end{pmatrix}, \quad \begin{pmatrix} \gamma_{xz} \\ \gamma_{yz} \end{pmatrix} = \begin{pmatrix} \phi_x + w_{,x} \\ \phi_y + w_{,y} \end{pmatrix}, \tag{5}$$

where

$$\begin{pmatrix} \varepsilon_x^0 \\ \varepsilon_y^0 \\ \gamma_{xy}^0 \end{pmatrix} = \begin{pmatrix} u_{,x} + w_{,x}^2/2 \\ v_{,y} - w/R + w_{,y}^2/2 \\ u_{,y} + v_{,x} + w_{,x}w_{,y} \end{pmatrix}, \quad \begin{pmatrix} \varepsilon_x^1 \\ \varepsilon_y^1 \\ \gamma_{xy}^1 \end{pmatrix} = \begin{pmatrix} \phi_{x,x} \\ \phi_{y,y} \\ \phi_{x,y} + \phi_{y,x} \end{pmatrix}, \tag{6}$$

in which u, v, w are displacement components of the middle plane in x, y, z directions, respectively, and ϕ_x, ϕ_y are rotations of a normal to the middle plane with respect to y, x axes, respectively.

The CNTRC sandwich panel is assumed to be thermal stress free at room temperature $T_0 = 300$ K and stress components are expressed as

$$\begin{pmatrix} \sigma_x \\ \sigma_y \\ \sigma_{xy} \\ \sigma_{xz} \\ \sigma_{yz} \end{pmatrix} = \begin{pmatrix} Q_{11} & Q_{12} & 0 & 0 & 0 \\ Q_{12} & Q_{22} & 0 & 0 & 0 \\ 0 & 0 & Q_{66} & 0 & 0 \\ 0 & 0 & 0 & Q_{44} & 0 \\ 0 & 0 & 0 & 0 & Q_{55} \end{pmatrix} \begin{pmatrix} \varepsilon_x - \alpha_{11}\Delta T \\ \varepsilon_y - \alpha_{22}\Delta T \\ \gamma_{xy} \\ \gamma_{xz} \\ \gamma_{yz} \end{pmatrix}, \tag{7}$$

where $\Delta T = T - T_0$ is uniform temperature rise from initial value T_0 and

$$Q_{11} = \frac{E_{11}}{1-\nu_{12}\nu_{21}}, Q_{22} = \frac{E_{22}}{1-\nu_{12}\nu_{21}}, Q_{12} = \frac{\nu_{21}E_{11}}{1-\nu_{12}\nu_{21}}, Q_{44} = G_{13}, Q_{55} = G_{23}, Q_{66} = G_{12}, \tag{8}$$

in CNTRC layers (i.e. $h_0 \le z \le h_1$ and $h_2 \le z \le h_3$ for sandwich panel of type A and $h_1 \le z \le h_2$ for sandwich panel of type B), and

$$\begin{aligned} &E_{11} = E_{22} = E_H, \quad \alpha_{11} = \alpha_{22} = \alpha_H, \quad \nu_{12} = \nu_{21} = \nu_H, \\ &Q_{11} = Q_{22} = \frac{E_H}{1-\nu_H^2}, \quad Q_{12} = \frac{\nu_H E_H}{1-\nu_H^2}, \quad Q_{44} = Q_{55} = Q_{66} = \frac{E_H}{2(1+\nu_H)}, \end{aligned} \tag{9}$$

in isotropic homogeneous layers (i.e. $h_0 \le z \le h_1$ and $h_2 \le z \le h_3$ for sandwich panel of type B and $h_1 \le z \le h_2$ for sandwich panel of type A) with E_H, α_H, ν_H are Young modulus, thermal expansion coefficient, Poisson ratio of isotropic homogeneous material, respectively.

Force and moment intensities per unit length of the panel are calculated through stress components as

$$\begin{aligned} &\left(N_x, N_y, N_{xy}\right) = \int_{-h/2}^{h/2} \left(\sigma_x, \sigma_y, \sigma_{xy}\right) \mathrm{d}z, \quad \left(M_x, M_y, M_{xy}\right) = \int_{-h/2}^{h/2} \left(\sigma_x, \sigma_y, \sigma_{xy}\right) z \mathrm{d}z, \\ &\left(Q_x, Q_y\right) = K_S \int_{-h/2}^{h/2} \left(\sigma_{xz}, \sigma_{yz}\right) \mathrm{d}z, \end{aligned} \tag{10}$$

in which K_S is shear correction coefficient assumed to be $5/6$ in the present work.

Based on the FSDT, system of equilibrium equations includes five equations and compact form of nonlinear equilibrium equation of geometrically perfect CNTRC sandwich cylindrical panel without external pressure is

$$a_{11}\phi_{x,xxx} + a_{21}\phi_{x,xyy} + a_{31}\phi_{y,xxy} + a_{41}\phi_{y,yyy} + a_{51}f_{,xxyy} + f_{,yy}w_{,xx} - 2f_{,xy}w_{,xy} + f_{,xx}w_{,yy} + \frac{f_{,xx}}{R} = 0, \tag{11}$$

where $f(x,y)$ is a stress function defined such that $N_x = f_{,yy}$, $N_y = f_{,xx}$, $N_{xy} = -f_{,xy}$, and

$$\begin{aligned} &a_{11} = e_{13} - \frac{e_{12}^2}{e_{11}}, \quad a_{21} = \nu_{12}e_{23} - \nu_{12}\frac{e_{22}^2}{e_{21}} + 2e_{33} - 2\frac{e_{32}^2}{e_{31}}, \\ &a_{31} = \nu_{21}e_{13} - \nu_{21}\frac{e_{12}^2}{e_{11}} + 2e_{33} - 2\frac{e_{32}^2}{e_{31}}, \quad a_{41} = e_{23} - \frac{e_{22}^2}{e_{21}}, \quad a_{51} = \frac{e_{12}}{e_{11}} - 2\frac{e_{32}}{e_{31}} + \frac{e_{22}}{e_{21}}, \end{aligned} \tag{12}$$

in which

$$\begin{aligned} \left(e_{11}, e_{21}, e_{31}\right) &= \int_{-h/2}^{h/2} \left(Q_{11}, Q_{22}, Q_{66}\right) \mathrm{d}z, \\ \left(e_{12}, e_{22}, e_{32}\right) &= \int_{-h/2}^{h/2} \left(Q_{11}, Q_{22}, Q_{66}\right) z \mathrm{d}z, \\ \left(e_{13}, e_{23}, e_{33}\right) &= \int_{-h/2}^{h/2} \left(Q_{11}, Q_{22}, Q_{66}\right) z^2 \mathrm{d}z. \end{aligned} \tag{13}$$

Next, strain compatibility equation of CNTRC sandwich cylindrical panel has the form

$$\begin{aligned} &a_{12}f_{,xxxx} + a_{22}f_{,xxyy} + a_{32}f_{,yyyy} + a_{42}\phi_{x,xxx} + a_{52}\phi_{y,xxy} \\ &\quad + a_{62}\phi_{y,yyy} + a_{72}\phi_{x,xyy} - w_{,xy}^2 + w_{,xx}w_{,yy} + \frac{w_{,xx}}{R} = 0, \end{aligned} \tag{14}$$

where coefficients a_{i2} $(i = 1 \div 7)$ can be found in the work [28].

The CNTRC sandwich cylindrical panel is assumed to be freely simply supported at all edges and subjected to axial compressive pressure P_x uniformly distributed on curved edges. The associated boundary conditions are expressed as

$$\begin{aligned} &w = \phi_y = N_{xy} = M_x = 0, \quad N_x = N_{x0} \quad \text{at } x = 0, a, \\ &w = \phi_x = N_{xy} = M_y = 0, \quad N_y = 0 \quad \text{at } y = 0, b, \end{aligned} \tag{15}$$

where $N_{x0} = -P_x h$ is pre-buckling force resultant at movable edges $x = 0, a$.

To satisfy boundary conditions (15), the following solutions are assumed

$$w = W \sin\beta_m x \sin\delta_n y, \tag{16a}$$

$$f = A_1 \cos 2\beta_m x + A_2 \cos 2\delta_n y + A_3 \sin\beta_m x \sin\delta_n y + \frac{1}{2}N_{x0}y^2, \tag{16b}$$

$$\phi_x = B_1 \cos\beta_m x \sin\delta_n y, \quad \phi_y = B_2 \sin\beta_m x \cos\delta_n y, \tag{16c}$$

where $\beta_m = m\pi/a$, $\delta_n = n\pi/b (m = 1, 2, \ldots)$, W is the amplitude of deflection, and A_1, A_2, A_3, B_1, B_2 are coefficients to be determined. By substituting solutions (16) into the compatibility equation (14) and two among five equilibrium equations, then following procedure described in the works [19,28,35], the coefficients A_i, B_j are determined as

$$\begin{aligned} &A_1 = \frac{\delta_n^2}{32a_{12}\beta_m^2}\left(W^2 + 2\mu h W\right), \quad A_2 = \frac{\beta_m^2}{32a_{32}\delta_n^2}\left(W^2 + 2\mu h W\right), \\ &B_1 = B_1^* W, \quad B_2 = B_2^* W, \quad A_3 = A_3^* W, \end{aligned} \tag{17}$$

where coefficients A_3^*, B_1^* and B_2^* have their forms as in the work [28].

Now, introduction of the solutions (16) into equilibrium equation (11) and applying Galerkin method to the resulting equation lead to the following relation

$$P_x = \frac{B_h^2}{m^2 B_a^2 \pi^2}\left[a_{13} + (a_{23} - a_{33})\overline{W} + a_{43}\overline{W}^2\right], \tag{18}$$

where

$$B_h = b/h, \quad B_a = b/a, \quad \overline{W} = W/h, \tag{19}$$

and coefficients a_{i3} $(i = 1 \div 4)$ have their forms similar to those in the work [28] and omitted here for the sake of brevity.

From Eq. (18), buckling compressive loads of CNTRC sandwich cylindrical panels are predicted as

$$P_{xb} = \frac{B_h^2 a_{13}}{m^2 B_a^2 \pi^2}, \tag{20}$$

and critical buckling compressive loads P_{xcr} are determined by minimizing P_{xb} with respect to numbers of half wave m, n.

4. RESULTS AND DISCUSSION

This section presents numerical results of buckling and postbuckling analyses for sandwich cylindrical panels in which nanocomposite layers are made of PMMA (Poly methyl methacrylate) matrix material and reinforced by $(10,10)$ single-walled carbon nanotubes (SWCNTs), and isotropic homogeneous layers are made of Ti-6Al-4V. The temperature dependent properties of the PMMA are assumed to be $\nu^m = 0.34$, $\alpha^m = 45\,(1+0.0005\Delta T)\times 10^{-6}\,\mathrm{K}^{-1}$ and $E^m = (3.52 - 0.0034T)$ GPa in which $T = T_0 + \Delta T$ and $T_0 = 300$ K (room temperature), whereas those of the Ti-6Al-4V are [33]

$$\begin{aligned} E_H &= 122.56\left(1 - 4.586\times 10^{-4}T\right)\ \text{GPa},\\ \alpha_H &= 7.5788\left(1 + 6.638\times 10^{-4}T - 3.147\times 10^{-7}T^2\right)\times 10^{-6}\,\mathrm{K}^{-1},\\ \nu_H &= 0.29. \end{aligned} \tag{21}$$

The temperature dependent properties of the $(10,10)$ SWCNTs are given in Tab. 1 and, by mathematical interpolation, as continuous functions of temperature in the works [13,23].

Table 1. Temperature-dependent material properties for $(10,10)$ SWCNT ($L^{CNT} = 9.26$ nm, $R^{CNT} = 0.68$ nm, $h^{CNT} = 0.067$ nm, $\nu_{12}^{CNT} = 0.175$) [14,20]

Temperature (K)	E_{11}^{CNT} (TPa)	E_{22}^{CNT} (TPa)	G_{12}^{CNT} (TPa)	$\alpha_{11}^{CNT}(\times 10^{-6}/\mathrm{K})$	$\alpha_{22}^{CNT}(\times 10^{-6}/\mathrm{K})$
300	5.6466	7.0800	1.9445	3.4584	5.1682
400	5.5679	6.9814	1.9703	4.1496	5.0905
500	5.5308	6.9348	1.9643	4.5361	5.0189
700	5.4744	6.8641	1.9644	4.6677	4.8943
1000	5.2814	6.6220	1.9451	4.2800	4.7532

Determining CNT efficiency parameters is key work for successful application of extended rule of mixture. For nanocomposite reinforced by $(10,10)$ SWCNTs, efficiency parameters are determined by matching results of effective elastic moduli obtained by rule of mixture and molecular dynamics simulation, and given in works [14, 22, 25] as $(\eta_1, \eta_2, \eta_3) = (0.137, 1.022, 0.715)$ for the case of $V_{CNT}^* = 0.12$, $(\eta_1, \eta_2, \eta_3) = (0.142, 1.626, 1.138)$ for the case of $V_{CNT}^* = 0.17$ and $(\eta_1, \eta_2, \eta_3) = (0.141, 1.585, 1.109)$ for the case of $V_{CNT}^* = 0.28$. In addition, it is assumed that $G_{13} = G_{12}$ and $G_{23} = 1.2G_{12}$ [14,33].

There is no result of buckling analysis for CNTRC sandwich cylindrical panels in the literature. Therefore, buckling behavior of a pure CNTRC cylindrical panel under axial compression with simply supported edges is considered for the sake of verification. Results of critical buckling loads of CNTRC cylindrical panels are obtained from Eq. (20) for a special case of sandwich model of type B as $h_f = 0$ and shown in Tab, 2 in comparison with results of Shen and Xiang [22] using asymptotic solutions and a perturbation technique. As can be seen, a good agreement is achieved in this comparison.

In what follows, buckling and posbuckling behaviors of CNTRC sandwich cylindrical panels of types A and B with square plan-form ($a = b$) will be analyzed. Tabs. 3 and 4

Table 2. Comparison of critical buckling loads $P_{xcr}bh$(kN) of perfect CNTRC cylindrical panels under uniform axial compression [$a/b = 0.98$, $a/R = 0.5$, $b/h = 20$, $h = 1$ mm, $(m,n) = (1,1)$]

V^*_{CNT}	Reference	UD	FG-X	FG-V
0.12	Ref. [22]	3.77[i] (3.45)[ii]	5.74 (5.34)	3.02 (2.74)
	Present	3.66 (3.43)	4.71 (4.38)	2.94 (2.74)
0.17	Ref. [22]	5.79 (5.29)	8.76 (8.14)	4.62 (4.16)
	Present	5.63 (5.29)	7.32 (6.84)	4.50 (4.21)
0.28	Ref. [22]	8.17 (7.58)	12.74 (11.94)	6.52 (6.04)
	Present	7.95 (7.43)	10.40 (9.65)	6.39 (6.00)

[i] $T = 300$ K, [ii] $T = 400$ K.

indicate the effects of CNT volume fraction V^*_{CNT}, distribution patterns and curvature ratio a/R on the critical buckling loads of CNTRC sandwich cylindrical panels of types A and B under axial compression.

Table 3. Critical buckling loads P_{xcr} (MPa) of sandwich cylindrical panels of type A under uniform axial compression [$a/b = 1$, $b/h = 25$, $h_f/h = 0.1$, $(m,n) = (1,1)$]

V^*_{CNT}	a/R	UD	FG-X	FG-V	FG-Λ
0.12	0.1	376.9 [i] (358.6 [ii])	377.1 (358.7)	381.3 (363.0)	372.5 (354.3)
	0.3	548.7 (521.3)	548.8 (521.4)	553.1 (525.7)	544.3 (517.0)
0.17	0.1	407.5 (388.3)	407.8 (388.6)	414.1 (394.8)	401.0 (382.0)
	0.3	581.2 (552.9)	581.5 (553.1)	587.8 (559.4)	574.8 (546.5)
0.28	0.1	461.3 (441.5)	462.1 (442.2)	472.5 (452.4)	451.2 (431.4)
	0.3	637.4 (608.3)	638.2 (609.0)	648.6 (619.2)	627.3 (598.3)

[i] $T = 300$ K, [ii] $T = 400$ K.

Table 4. Critical buckling loads P_{xcr} (MPa) of sandwich cylindrical panels of type B under uniform axial compression [$a/b = 1$, $b/h = 25$, $h_f/h = 0.1$, $(m,n) = (1,1)$]

V^*_{CNT}	a/R	UD	FG-X	FG-V	FG-Λ
0.12	0.1	345.5 [i] (328.8 [ii])	375.6 (358.4)	335.4 (318.5)	327.2 (310.7)
	0.3	396.3 (376.6)	426.4 (406.2)	394.4 (374.1)	369.8 (350.8)
0.17	0.1	376.9 (359.3)	421.3 (402.8)	358.8 (341.0)	349.5 (332.1)
	0.3	430.8 (409.8)	475.3 (453.5)	422.2 (400.5)	394.1 (373.9)
0.28	0.1	430.9 (412.5)	502.9 (483.0)	396.7 (378.2)	386.4 (368.5)
	0.3	486.2 (464.2)	558.6 (535.1)	462.6 (439.9)	431.8 (410.9)

[i] $T = 300$ K, [ii] $T = 400$ K.

For sandwich panels of the type A with CNTRC face sheets, Tab. 3 shows that CNT distribution has slight effects on the critical loads. Specifically, FG-V and FG-Λ panels have slightly higher and lower values of critical loads, respectively, and critical loads corresponding to UD and FG-X panels are almost coincided.

For sandwich panels of type B with CNTRC core layer, Tab. 4 demonstrates that CNT distribution type has significant effects on the critical loads, especially for higher values of CNT volume fraction. More specifically, FG-X and FG-Λ panels have the highest and lowest critical loads, respectively, and UD type results in average critical loads of CNTRC sandwich panels. Furthermore, it is recognized from Tabs. 3 and 4 that, for both types of sandwich panels, critical loads are pronouncedly increased as CNT volume fraction and/or curvature of panels are increased, and decreased when the panels are exposed to elevated temperature.

The postbuckling behavior of CNTRC sandwich cylindrical panels of types A and B under axial compression are graphically analyzed in Figs. 4–8.

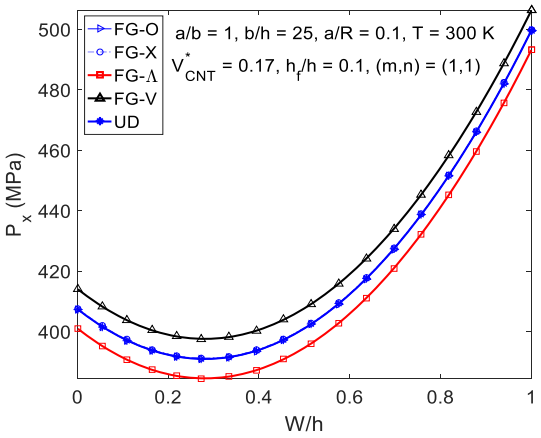

Fig. 4. Effects of CNT distribution patterns on the postbuckling behavior of sandwich cylindrical panel with CNTRC face sheets under axial compression

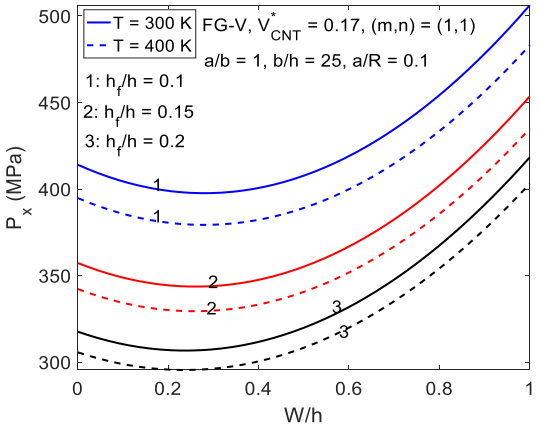

Fig. 5. Effects of h_f/h ratio on the postbuckling behavior of sandwich cylindrical panel with CNTRC face sheets under axial compression

Figs. 4 and 5 show the effects of CNT distribution patterns, thickness of face sheet-to-total thickness h_f/h ratio and environment temperature T on the postbuckling behavior of sandwich panels of type A with CNTRC face sheets. It is evident from Fig. 4 that FG-V and FG-Λ panels have the strongest and weakest postbuckling strengths, respectively, and UD, FG-X and FG-O panels have intermediate and almost identical postbuckling curves. Subsequently, it is realized from Fig. 5 that critical loads and postbuckling paths are significantly reduced when h_f/h ratio is enhanced, especially as h_f/h increases from 0.1 to 0.15. In addition, the load carrying capability of sandwich panels is decreased at elevated temperature ($T = 400$ K) and detrimental effect of temperature is more pronounced for smaller values of h_f/h ratio.

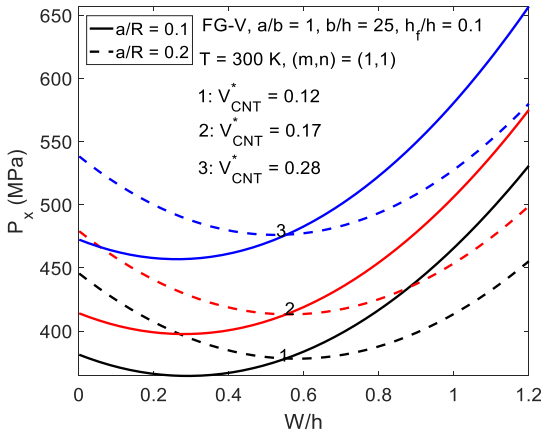

Fig. 6. Effects of V^*_{CNT} and a/R ratio on the postbuckling behavior of sandwich cylindrical panel with CNTRC face sheets under axial compression

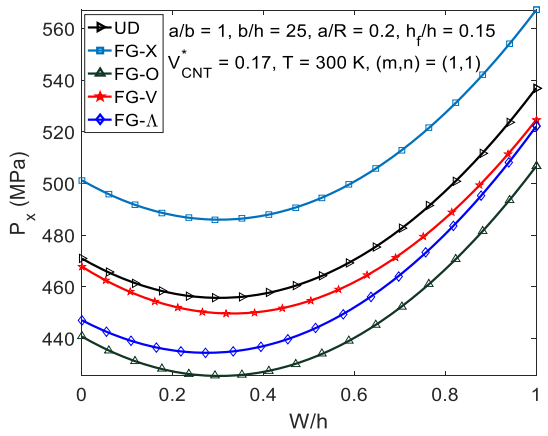

Fig. 7. Effects of CNT distribution patterns on the postbuckling behavior of sandwich cylindrical panel with CNTRC core layer under axial compression

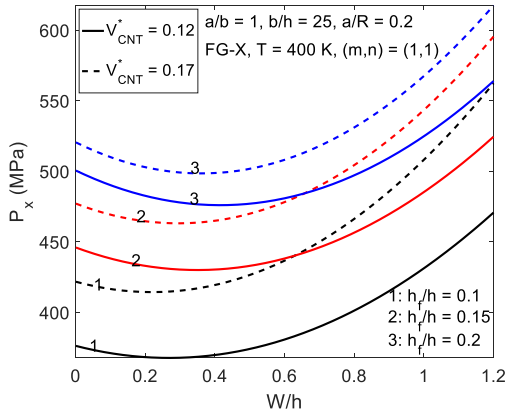

Fig. 8. Effects of thickness of face sheets on the postbuckling behavior of sandwich cylindrical panel with CNTRC core layer under axial compression in a thermal environment

As a subsequent example, the influences of curvature ratio a/R and CNT volume fraction V^*_{CNT} on the postbuckling behavior of sandwich panels with CNTRC face sheets are examined in Fig. 6. Obviously, the critical buckling loads and postbuckling equilibrium paths are considerably enhanced when a/R and/or V^*_{CNT} are increased. In other words, more curved and CNT-rich panels have higher postbuckling paths. However, more curved panels ($a/R = 0.2$) experience an unstable postbuckling response with relatively intense snap-through instability.

Next, numerical illustrations on the postbuckling behavior of sandwich panels of type B with CNTRC core layer and homogeneous face sheets under axial compression are given in Figs. 7 and 8. Fig. 7 indicates that distribution patterns of CNTs in the core

layer have significant effects on the postbuckling response of sandwich panels of type B. Specifically, among five distribution types, FG-X and FG-O types give the best and worst postbuckling response, respectively, and UD panel has higher postbuckling strength than FG-V panel, especially in the deep region of deflection.

Finally, the interactive effects of h_f/h ratio and CNT volume fraction V^*_{CNT} on the postbuckling behavior of sandwich panels of type B in a thermal environment ($T = 400$ K) are considered in Fig. 8. It is clear that buckling loads and postbuckling paths are remarkably enhanced due to increase in h_f/h ratio. In addition, effects of CNT volume fraction are more slight for larger values of h_f/h ratio, i.e. thicker face sheets.

5. CONCLUDING REMARKS

An analytical investigation on the buckling and postbuckling behaviors of two models of sandwich cylindrical panels comprising CNTRC and homogeneous layers and subjected to uniform axial compression in thermal environments has been presented. From the above results, the following remarks are reached:

1. For sandwich panels of type A with CNTRC face sheets, the type of CNT distribution has relatively slight effects on the critical loads and postbuckling equilibrium paths of sandwich panels. In this configuration of sandwich panels, FG-V and FG-Λ types give the highest and lowest postbuckling strengths, respectively, and load carrying capability of the panel is reduced as thickness of face sheets is increased.

2. For sandwich panels of type B with CNTRC core layer, the type of CNT distribution has significant effects on the critical loads and postbuckling equilibrium paths of sandwich panels, and FG-X and FG-O distributions give the best and worst postbuckling responses of sandwich panels, respectively. For this sandwich model, the load carrying capability of the panel is enhanced when the thickness of face sheets is increased.

3. For both models of sandwich cylindrical panels, postbuckling load-deflection paths are enhanced and reduced due to increase in the volume fraction of CNTs and environment temperature, respectively.

ACKNOWLEDGMENT

This research is funded by Vietnam National Foundation for Science and Technology Development (NAFOSTED) under grant number 107.02-2017.11.

REFERENCES

[1] E. T. Thostenson, Z. Ren, and T. W. Chou. Advances in the science and technology of carbon nanotubes and their composites: a review. *Composites Science and Technology*, **61**, (13), (2001), pp. 1899–1912. https://doi.org/10.1016/s0266-3538(01)00094-x.

[2] E. T. Thostenson, C. Li, and T. W. Chou. Nanocomposites in context. *Composites Science and Technology*, **65**, (3-4), (2005), pp. 491–516. https://doi.org/10.1016/j.compscitech.2004.11.003.

[3] J. N. Coleman, U. Khan, W. J. Blau, and Y. K. Gunko. Small but strong: a review of the mechanical properties of carbon nanotube–polymer composites. *Carbon*, **44**, (9), (2006), pp. 1624–1652. https://doi.org/10.1016/j.carbon.2006.02.038.

[4] O. Gohardani, M. C. Elola, and C. Elizetxea. Potential and prospective implementation of carbon nanotubes on next generation aircraft and space vehicles: A review of current and expected applications in aerospace sciences. *Progress in Aerospace Sciences*, **70**, (2014), pp. 42–68. https://doi.org/10.1016/j.paerosci.2014.05.002.

[5] H. S. Shen. Nonlinear bending of functionally graded carbon nanotube-reinforced composite plates in thermal environments. *Composite Structures*, **91**, (1), (2009), pp. 9–19. https://doi.org/10.1016/j.compstruct.2009.04.026.

[6] Z. X. Lei, K. M. Liew, and J. L. Yu. Buckling analysis of functionally graded carbon nanotube-reinforced composite plates using the element-free kp-Ritz method. *Composite Structures*, **98**, (2013), pp. 160–168. https://doi.org/10.1016/j.compstruct.2012.11.006.

[7] L. W. Zhang, Z. X. Lei, and K. M. Liew. An element-free IMLS-Ritz framework for buckling analysis of FG–CNT reinforced composite thick plates resting on Winkler foundations. *Engineering Analysis with Boundary Elements*, **58**, (2015), pp. 7–17. https://doi.org/10.1016/j.enganabound.2015.03.004.

[8] Z. X. Lei, L. W. Zhang, and K. M. Liew. Buckling analysis of CNT reinforced functionally graded laminated composite plates. *Composite Structures*, **152**, (2016), pp. 62–73. https://doi.org/10.1016/j.compstruct.2016.05.047.

[9] Z. X. Lei, L. W. Zhang, and K.-M. Liew. Buckling of FG-CNT reinforced composite thick skew plates resting on Pasternak foundations based on an element-free approach. *Applied Mathematics and Computation*, **266**, (2015), pp. 773–791. https://doi.org/10.1016/j.amc.2015.06.002.

[10] Y. Kiani. Shear buckling of FG-CNT reinforced composite plates using Chebyshev-Ritz method. *Composites Part B: Engineering*, **105**, (2016), pp. 176–187. https://doi.org/10.1016/j.compositesb.2016.09.001.

[11] Y. Kiani. Buckling of FG-CNT-reinforced composite plates subjected to parabolic loading. *Acta Mechanica*, **228**, (4), (2017), pp. 1303–1319. https://doi.org/10.1007/s00707-016-1781-4.

[12] Y. Kiani and M. Mirzaei. Rectangular and skew shear buckling of FG-CNT reinforced composite skew plates using Ritz method. *Aerospace Science and Technology*, **77**, (2018), pp. 388–398. https://doi.org/10.1016/j.ast.2018.03.022.

[13] M. Mirzaei and Y. Kiani. Thermal buckling of temperature dependent FG-CNT reinforced composite plates. *Meccanica*, **51**, (9), (2016), pp. 2185–2201. https://doi.org/10.1007/s11012-015-0348-0.

[14] H. S. Shen and C. L. Zhang. Thermal buckling and postbuckling behavior of functionally graded carbon nanotube-reinforced composite plates. *Materials & Design*, **31**, (7), (2010), pp. 3403–3411. https://doi.org/10.1016/j.matdes.2010.01.048.

[15] Y. Kiani. Thermal post-buckling of FG-CNT reinforced composite plates. *Composite Structures*, **159**, (2017), pp. 299–306. https://doi.org/10.1016/j.compstruct.2016.09.084.

[16] L. W. Zhang and K. M. Liew. Postbuckling analysis of axially compressed CNT reinforced functionally graded composite plates resting on Pasternak foundations using an element-free approach. *Composite Structures*, **138**, (2016), pp. 40–51. https://doi.org/10.1016/j.compstruct.2015.11.031.

[17] H. V. Tung. Thermal buckling and postbuckling behavior of functionally graded carbon-nanotube-reinforced composite plates resting on elastic foundations with tangential-edge restraints. *Journal of Thermal Stresses*, **40**, (5), (2017), pp. 641–663. https://doi.org/10.1080/01495739.2016.1254577.

[18] L. T. N. Trang and H. V. Tung. Tangential edge constraint sensitivity of nonlinear stability of CNT-reinforced composite plates under compressive and thermomechanical loadings. *Journal of Engineering Mechanics*, **144**, (7), (2018). https://doi.org/10.1061/(asce)em.1943-7889.0001479.

[19] H. V. Tung and L. T. N. Trang. Thermal postbuckling of shear deformable CNT-reinforced composite plates with tangentially restrained edges and temperature-dependent properties. *Journal of Thermoplastic Composite Materials*, (2018). https://doi.org/10.1177/0892705718804588.

[20] E. García-Macías, L. Rodriguez-Tembleque, R. Castro-Triguero, and A. Sáez. Buckling analysis of functionally graded carbon nanotube-reinforced curved panels under axial compression and shear. *Composites Part B: Engineering*, **108**, (2017), pp. 243–256. https://doi.org/10.1016/j.compositesb.2016.10.002.

[21] E. García-Macías, L. Rodríguez-Tembleque, R. Castro-Triguero, and A. Sáez. Eshelby-Mori-Tanaka approach for post-buckling analysis of axially compressed functionally graded CNT/polymer composite cylindrical panels. *Composites Part B: Engineering*, **128**, (2017), pp. 208–224. https://doi.org/10.1016/j.compositesb.2017.07.016.

[22] H. S. Shen and Y. Xiang. Postbuckling of axially compressed nanotube-reinforced composite cylindrical panels resting on elastic foundations in thermal environments. *Composites Part B: Engineering*, **67**, (2014), pp. 50–61. https://doi.org/10.1016/j.compositesb.2014.06.020.

[23] H. S. Shen. Postbuckling of nanotube-reinforced composite cylindrical panels resting on elastic foundations subjected to lateral pressure in thermal environments. *Engineering Structures*, **122**, (2016), pp. 174–183. https://doi.org/10.1016/j.engstruct.2016.05.004.

[24] H. S. Shen and Y. Xiang. Thermal postbuckling of nanotube-reinforced composite cylindrical panels resting on elastic foundations. *Composite Structures*, **123**, (2015), pp. 383–392. https://doi.org/10.1016/j.compstruct.2014.12.059.

[25] H. S. Shen and Y. Xiang. Nonlinear response of nanotube-reinforced composite cylindrical panels subjected to combined loadings and resting on elastic foundations. *Composite Structures*, **131**, (2015), pp. 939–950. https://doi.org/10.1016/j.compstruct.2015.06.042.

[26] H. V. Tung and L. T. N. Trang. Imperfection and tangential edge constraint sensitivities of thermomechanical nonlinear response of pressure-loaded carbon nanotube-reinforced composite cylindrical panels. *Acta Mechanica*, **229**, (5), (2018), pp. 1949–1969. https://doi.org/10.1007/s00707-017-2093-z.

[27] L. T. N. Trang and H. V. Tung. Thermomechanical nonlinear analysis of axially compressed carbon nanotube-reinforced composite cylindrical panels resting on elastic foundations with tangentially restrained edges. *Journal of Thermal Stresses*, **41**, (4), (2018), pp. 418–438. https://doi.org/10.1080/01495739.2017.1409093.

[28] L. T. N. Trang and H. V. Tung. Nonlinear stability of CNT-reinforced composite cylindrical panels with elastically restrained straight edges under combined thermomechanical loading conditions. *Journal of Thermoplastic Composite Materials*, (2018). https://doi.org/10.1177/0892705718805134.

[29] Z. X. Wang and H. S. Shen. Nonlinear vibration and bending of sandwich plates with nanotube-reinforced composite face sheets. *Composites Part B: Engineering*, **43**, (2), (2012), pp. 411–421. https://doi.org/10.1016/j.compositesb.2011.04.040.

[30] M. Wang, Z. M. Li, and P. Qiao. Vibration analysis of sandwich plates with carbon nanotube-reinforced composite face-sheets. *Composite Structures*, **200**, (2018), pp. 799–809. https://doi.org/10.1016/j.compstruct.2018.05.058.

[31] K. Mehar, S. K. Panda, and T. R. Mahapatra. Thermoelastic nonlinear frequency analysis of CNT reinforced functionally graded sandwich structure. *European Journal of Mechanics-A/Solids*, **65**, (2017), pp. 384–396. https://doi.org/10.1016/j.euromechsol.2017.05.005.

[32] H. S. Shen and Z. H. Zhu. Postbuckling of sandwich plates with nanotube-reinforced composite face sheets resting on elastic foundations. *European Journal of Mechanics-A/Solids*, **35**, (2012), pp. 10–21. https://doi.org/10.1016/j.euromechsol.2012.01.005.

[33] Y. Kiani. Thermal post-buckling of temperature dependent sandwich plates with FG-CNTRC face sheets. *Journal of Thermal Stresses*, **41**, (7), (2018), pp. 866–882. https://doi.org/10.1080/01495739.2018.1425645.

[34] V. T. Long and H. V. Tung. Thermal postbuckling behavior of CNT-reinforced composite sandwich plate models resting on elastic foundations with tangentially restrained edges and temperature-dependent properties. *Journal of Thermoplastic Composite Materials*, (2019). https://doi.org/10.1177/0892705719828789.

[35] V. T. Long and H. V. Tung. Thermomechanical postbuckling behavior of CNT-reinforced composite sandwich plate models resting on elastic foundations with elastically restrained unloaded edges. *Journal of Thermal Stresses*, **42**, (5), (2019), pp. 658–680. https://doi.org/10.1080/01495739.2019.1571972.

[36] L. T. N. Trang and H. V. Tung. Buckling and postbuckling of carbon nanotube-reinforced composite cylindrical panels subjected to axial compression in thermal environments. *Vietnam Journal of Mechanics*, **40**, (1), (2018), pp. 47–61. https://doi.org/10.15625/0866-7136/10088.

[37] H. V. Tung and P. T. Hieu. Buckling and postbuckling of axially-loaded CNT-reinforced composite cylindrical shell surrounded by an elastic medium in thermal environment. *Vietnam Journal of Mechanics*, **41**, (1), (2019), pp. 31–49. https://doi.org/10.15625/0866-7136/12602.